Quantitative analysis of changes in spatial distribution and plus-end geometry of microtubules involved in plant-cell cytokinesis

Jotham R. Austin, II*, José M. Seguí-Simarro and L. Andrew Staehelin

Department of Molecular, Cellular and Developmental Biology, University of Colorado, UCB 347, Boulder, CO 80309-0347, USA

*Author for correspondence (e-mail: jotham.austinii@colorado.edu)

Accepted 25 May 2005
Journal of Cell Science 118, 3895-3903 Published by The Company of Biologists 2005
doi:10.1242/jcs.02512

Summary

The cell plate of higher plants is formed within a ribosome-excluding cell plate assembly matrix. Phragmoplast microtubules facilitate cell-plate formation by forming a scaffold that directs Golgi-derived vesicles to the forming cell plate. Here, we analyse the effects of the cell-plate assembly matrix on phragmoplast microtubule plus-end geometry by electron tomography of cryogenically fixed *Arabidopsis* meristem cells. Five distinct microtubules plus-end geometries are seen – blunt, extended, horned, flared and hybrid extended/horned. We have quantified and mapped these types of plus-end morphology during the different stages of cell-plate formation and analysed the effects of cell-plate assembly matrix association on microtubule plus-end morphologies. Our results show that somatic-type phragmoplast microtubules do not interdigitate at the cell plate mid-line. The cell-plate assembly matrix is shown to stabilize microtubule plus ends, as evidenced by the fact that of these microtubules that do not terminate in such a matrix, 40-80% are horn-shaped (shrinking), whereas of those that end in such a matrix, 50-70% are blunt (metastable). Also, a third of the blunt-ended microtubules within the cell-plate assembly matrix end at a distance of ~30 nm from the cell plate.

Key words: *Arabidopsis*, Phragmoplast, Microtubule dynamics, Electron tomography, 3D tomography

Introduction

Plant cells divide by forming a new cell wall between the two daughter cells (Verma, 2001; Mayer and Jürgens, 2004). This wall derives from a transient membranous structure, the cell plate, which is formed by a cytoskeletal array known as the phragmoplast. The phragmoplast is composed of two opposing sets of microtubules and actin filaments as well as the ribosome-excluding cell-plate assembly matrix within which the cell plate is formed (Lambert, 1993; Staehelin and Hepler, 1996; Otegui et al., 2001; Wasteneys, 2002; Seguí-Simarro et al., 2004). The microtubule plus ends face the cell plate (Euteneuer et al., 1982) and most terminate within the cell-plate assembly matrix (Seguí-Simarro et al., 2004). It is widely assumed that somatic-type phragmoplast microtubules interdigitate at the mid-line of the cell plate (Raven et al., 1999; Alberts et al., 2004; Müller et al., 2004; Smerteneko et al., 2004; Van Damme et al., 2004), even though many studies do not support this assumption (Pickett-Heaps and Northcote, 1966; Whaley et al., 1966; Hepler and Newcomb, 1967; Samuels et al., 1995).

The formation of a new cell wall is a multistep process, with each step being defined by the organization of the phragmoplast and the architecture of the cell-plate intermediates (Samuels et al., 1995; Seguí-Simarro et al., 2004). The principle stages are as follows. (1) Phragmoplast assembly. During this stage, the phragmoplast initials arise from opposite sets of polar spindle microtubules, and then enlarge by lateral expansion. This stage also involves the transport of Golgi-derived vesicles and preassembled cell-plate assembly matrix along the microtubules to the future site of cell-plate assembly. (2) Solid phragmoplast. This stage is defined by a continuous cell-plate assembly matrix that extends across the phragmoplast region and two massive and opposing arrays of microtubules. (3) Transitional phragmoplast. During this stage, the cell-plate assembly matrix and microtubules of the solid phragmoplast are disassembled and new ones appear at the edge of the cell plate, creating the ring phragmoplast. (4) Ring-shaped phragmoplast. This stage is defined by a ring-shaped peripheral cell-plate assembly matrix with associated microtubules, which is responsible for the centrifugal cell-plate growth that continues until the cell plate fuses with the parent cell wall (Samuels et al., 1995; Seguí-Simarro et al., 2004).

During the past 40 years, the phragmoplast microtubule array has been studied by a range of light- and electron-microscopic techniques (Pickett-Heaps and Northcote, 1966; Whaley et al., 1966; Hepler and Newcomb, 1967; Bajer, 1968; Hepler and Jackson, 1968; Gunning and Steer, 1975; Wick, 1985; Samuels et al., 1995; Staehelin and Hepler, 1996; Granger and Cyr, 2000; Seguí-Simarro et al., 2004; Mayer and Jürgens, 2004). The most informative have been studies in which fluorescent brain tubulin was microinjected into living plant cells (Zhang et al., 1990; Hush et al., 1994). These investigations demonstrated that the phragmoplast microtubule array is highly dynamic and, based on fluorescence

redistribution after photobleaching experiments, a microtubule turnover rate of $t_{½}$=60 seconds was determined (Hush et al., 1994).

Efforts to understand the molecular basis of microtubule turnover have included in vitro studies of growing and shrinking microtubules in which the samples were cryogenically fixed and examined in the frozen state in a cryoelectron microscope (Mandelkow et al., 1991; Chrétien et al., 1995; Arnal et al., 2000; Carvalho et al., 2003). This experimental approach led to the identification of three different types of microtubule plus-end morphologies: (1) extended ends, which are typical of growing microtubules; (2) ram's-horn-like ends, which are characteristic of disassembling microtubules; and (3) blunt ends, which reflect a metastable state. More recently, a fourth microtubule plus-end morphology, flared, has been identified in electron-tomographic studies of the mitotic kinetochores of *Caenorhabditis elegans* (O'Toole et al., 2003). To date, no systematic studies of microtubule plus-end geometries have been reported in plants.

Here, we demonstrate that electron tomography can resolve five different types of phragmoplast microtubule plus ends in plant cells and that association of these ends with the cell-plate assembly matrix has a profound effect on relative frequencies of the different types of plus-end morphologies. Finally, we provide evidence that about one-third of the blunt-ended phragmoplast microtubules terminate within ~30 nm of the cell plate.

Materials and Methods

Plant material

Seeds of *Arabidopsis thaliana* (Landsberg *erecta* wild type) were planted in 0.8% (w/v) agar plates with MS (Murashige & Skoog) medium with 1% sucrose for 5 days. Seedlings were grown at a temperature of 24°C, a light intensity of 150 μM photons m^{-2} s^{-1} and a photoperiod of 16 hours light/8 hours dark.

Sample preparation for electron tomography

Shoot or root apical meristems were excised from 5-day-old seedlings and transferred to aluminum sample holders, cryoprotected with 150 mM sucrose and frozen in a Baltec HPM 010 high-pressure freezer (Technotrade, Manchester, NH). Samples were then freeze substituted in 4% OsO_4 (shoot meristems) or 2% OsO_4 (root meristems) in anhydrous acetone at –80°C for 5 days, followed by slow warming to room temperature over a period of 2 days, removed from the holders and infiltrated with increasing concentrations of Epon (Ted Pella, Redding, CA). Polymerization was carried out at 60°C for 2 days under vacuum. Epon (250-450 nm thick) sections were prepared for electron tomography as described by Otegui et al. (Otegui et al., 2001).

Intermediate/high-voltage electron microscopy and acquisition of tilt series images

Three tomograms were collected on a FEI Tecnai TF30 intermediate-voltage electron microscope (FEI, Hiilsboro, OR, USA) operating at 300 kV. The images were taken at 20,000× from +60° to –60° at 1° intervals about two orthogonal axes (Ladinsky et al., 1997), being collected with a Gatan Megascan 795 digital camera (Gatan, Pleasanton, CA, USA) that covered a 2.6 μm × 2.6 μm region and had a resolution of 2048×2048 pixels at a pixel size of 1.26 nm. The remaining tomograms where collected on a JEM-1000 high-voltage electron microscope (JEOL, Akishima, Tokyo, Japan) operating at 750 kV. The images were collected as described by Seguí-Simarro et al. (Seguí-Simarro et al., 2004). For the large tomograms (using either the FEI Tecnai TF30 or the Jem-1000 HVEM), single images of adjacent frames (two to 16) were combined into montaged tilt series (Marsh et al., 2001).

Three-dimensional tomographic reconstruction, modeling and analysis

The images (single or montaged frames) were aligned using the gold particles as reference markers as described previously (Ladinsky et al., 1999). Each set of aligned tilts was reconstructed into a single-axis tomogram using the *R*-weighted back-projection algorithm (Gilbert, 1972). Merging the two single-axis tomograms into a dual-axis tomogram involved a warping procedure rather than a single linear transformation producing the dual-axis tomogram (Mastronarde, 1997). In addition, dual-axis tomograms computed from adjacent serial sections were aligned and joined to increase the reconstructed volume (Otegui et al., 2001). Tomograms were displayed and analysed with 3dmod, the graphics component of the 3DMOD (formerly Imod) software package (Kremer et al., 1996). Membranous structures, microtubules and all types of vesicles were modeled as described previously (Marsh et al., 2001). Once a model was completed, meshes of triangles were computed to define the surface of each object (Kremer et al., 1996).

The 'image slicer' tool of 3dmod was used to display and analyse tomographic slices extracted from the tomogram in any position or tilt around the *x*, *y* or *z* axes. This tool allowed us to obtain squeezed images in which several consecutive 2.2 nm tomographic slices were combined, thus generating *z*-axis projections of different thickness, more similar to conventional electron-microscopic thin sections. This tool was also particularly useful for modeling and identifying the different geometries of microtubule plus ends.

The spatial relationship between microtubule plus ends to the cell-plate membrane was determined by measuring the distances between the objects in three dimensions and computing an average density of neighboring items as a function of distance between objects using the MTK program (Kremer et al., 1996; Marsh et al., 2001). Distances were measured from the central axis of the microtubule plus end to the surface of the cell-plate membrane. The bar graphs depict the actual spatial relationship between the microtubule plus end and the surface of the cell-plate membrane. The line on each of these graphs compares the distances between randomly arranged microtubule plus ends and the cell-plate membrane. This random distribution was obtained by shifting the microtubule plus ends to new positions within the three-dimensional (3D) volume of the modeled cell-plate assembly matrix and rejected positions that shifted outside the modeled region or that resulted in collisions between objects (Marsh et al., 2001; O'Toole et al., 2003). This is the standard way to determine whether a distribution of items is non-random, and the graph compares the density distribution of the randomly shifted microtubules to those in the actual model.

Results

To identify positively the different stages of the mitotic and phragmoplast microtubule arrays analysed in this study, we have created large-volume tomographic reconstructions of cryogenically fixed meristem cells (Fig. 1). These reconstructions have enabled us to analyse close to 1000 individual microtubules from end to end (minus end adjacent to the nucleus, plus ends facing the cell-plate region). We were able unambiguously to classify the plus ends of 846 of these microtubules, from 16 different cells (three different cells from each stage represented in Fig. 1, except the solid phragmoplast

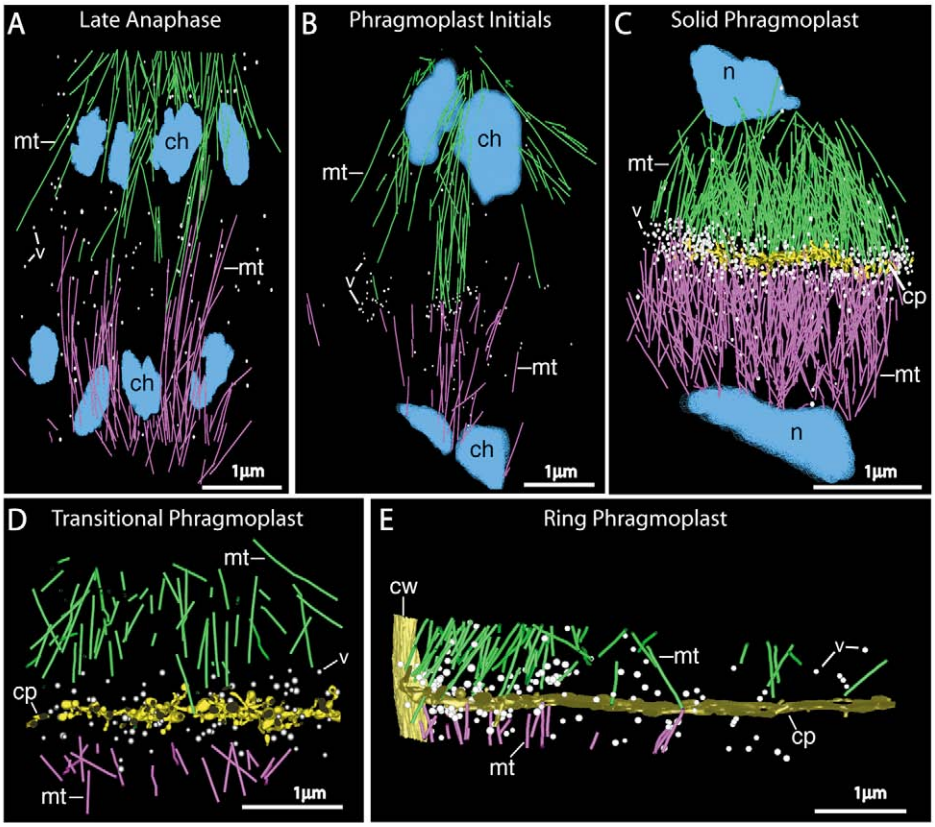

Fig. 1. Large-volume tomographic reconstructions of different stages of mitosis and cytokinesis in *Arabidopsis* meristem cells. All of the tomographic models are cells from root meristems, except the ring phragmoplast stage, which is from an apical-meristem cell. (A) Late-anaphase (5.9×5.9×0.8 μm), which shows two opposing sets of spindle microtubules (mt; green and pink) above and between the migrating sister chomatids (ch) and vesicles (v). (B) Phragmoplast initials (5.9×5.9×0.8 μm) in which the phragmoplast microtubule array is beginning to form between the decondensing chromatin, and cell-plate-forming vesicles and cell-plate assembly matrix (not shown) accumulate at the equatorial plane. (C) Solid-phragmoplast stage (4.3×4.3×1.2 μm), with two dense sets of opposing microtubules between the forming daughter nuclei (n). The growing cell plate (cp) is surrounded by many vesicles and is sandwiched between the two sets of microtubules. (D) Transitional-phragmoplast stage (2.8×2.8×0.8 μm), which lacks a cell-plate assembly matrix and displays many short microtubules on both sides of the maturing cell plate. (E) Ring-phragmoplast stage (5.9×2.8×0.9 μm). Two dense sets of opposing microtubules flank the growing edge of cell plate, which is surrounded by many vesicles, and a cell-plate assembly matrix (not shown). The more mature central cell-plate region has fewer interacting microtubules. Scale bars, 1 μm.

stage were four cells were examined). The remaining plus ends could not be classified unambiguously because they either terminated in the blurred interface regions of the serial sections or stained irregularly. The models also demonstrate that, during somatic-type cytokinesis, the microtubule plus ends do not interdigitate at the cell-plate mid-line (Fig. 1B-E).

Five types of phragmoplast microtubule plus-end morphology

The tomograms produced during this study yielded calculated slices with a thickness of 2.2 nm. This slice thickness enabled us to resolve each 25 nm diameter microtubule into 12 longitudinal serial slices, which was sufficient to resolve the geometry of the microtubule plus ends (Fig. 2A). Notice that, in Fig. 2A, a horned microtubule end depicts only every third 2.2 nm slice image. By carefully tracing the end structures of each microtubule in all 12 slices, it became possible to produce best-fit reconstructions of microtubule end morphologies (Fig. 2B-M). However, because the diameter of the microtubule protofilaments (4 nm) is smaller than the 3D resolution of our samples (5-7 nm), the filamentous structures shown in our reconstructions do not correspond exactly to individual microtubule protofilaments. Nevertheless, the resolution of the high-pressure-frozen, freeze-substituted and plastic-embedded samples is clearly sufficient for distinguishing the five types of microtubule plus-end morphologies, which was observed in all stages. The five identifiable types of microtubule plus-end geometries are: (1) blunt (Fig. 2B-D); (2) extended (Fig. 2E-G); (3) horned (Fig. 2H-I); (4) flared (Fig. 2K-M); and (5) hybrid horned/extended (Fig. 2J). The blunt-ended microtubules have protofilaments that are parallel with each other up to the microtubule end and are approximately of equal length (Fig. 2B-D′). Microtubules with extended ends exhibit a sheet-like organization of slightly curved, laterally associated protofilaments that extend from one side of the microtubule and range in length from 50 nm to 300 nm (Fig. 2E-G′). Microtubules with horn-shaped ends have splayed protofilaments that curl away from the microtubule end (Fig. 2H-I′). Microtubules with flared ends (Fig. 2K-M′) are seen rather infrequently (1-2% of the total microtubule population). The least frequently (<1%) observed type of microtubule plus end is the hybrid horned/extended end (Fig. 2J,J′).

Cell-plate assembly matrix, cell-plate membrane and microtubule plus ends

We have previously reported that most phragmoplast microtubules terminate within the cell-plate assembly matrix (Seguí-Simarro et al., 2004). Here, we demonstrate that this association has a profound effect on microtubule plus-end morphology (Figs 3, 4). To analyse the cell-plate assembly matrix effects on microtubule plus ends, we have taken advantage of the fact that, at different stages of cell-plate formation, the proportion of microtubules associated with the

cell-plate assembly matrix varies. Thus, as the phragmoplast array matures from the initial stage to the solid-phragmoplast stage (Fig. 1B,C), the proportion of microtubules that terminate in the cell-plate assembly matrix increases from 30% to 65%. By contrast, during the transformation of the solid phragmoplast to a transitional phragmoplast (Fig. 1C,D), the proportion drops from 65% to 0%.

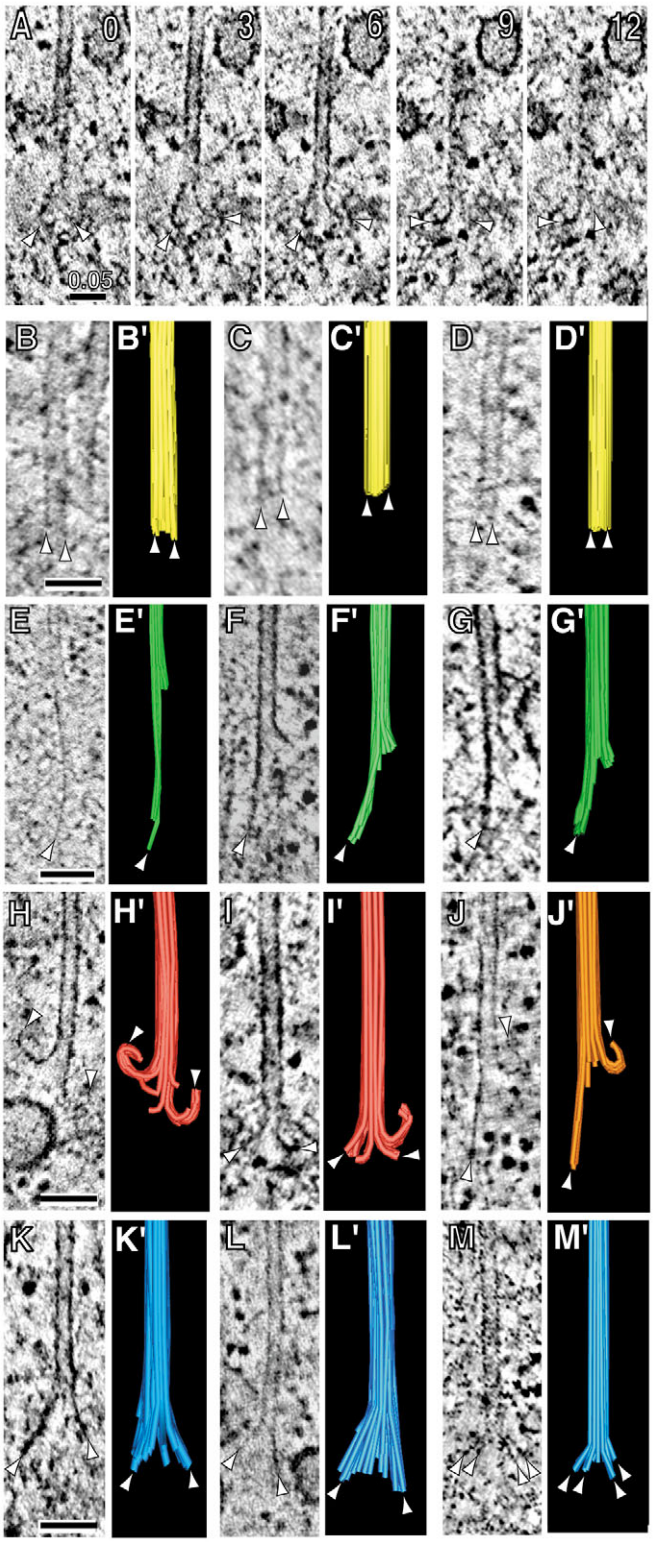

The effect of cell-plate assembly matrix association on microtubule plus ends is illustrated graphically in Fig. 3 and quantitatively in Fig. 4. In Fig. 3, the microtubule plus-end types are shown as colored dots (yellow, blunt ends; green, extended ends; red, horned ends; blue, flared ends). The high proportion of yellow dots associated with the solid phragmoplast cell-plate assembly matrix (Fig. 3B) illustrates that the association of a microtubule plus end with the cell-plate assembly matrix increases its probability of becoming blunt ended. The proportion of blunt-ended microtubules in this sample is ~70% and the proportions of extended and horned microtubule plus ends are each 15-20% (Fig. 4B). By contrast, of those microtubules that terminate outside the cell-plate assembly matrix in this solid phragmoplast, only ~20% of their plus ends are blunt, whereas ~45% are extended and ~35% horned (Fig. 4C). The cell-plate assembly matrix breaks down during the transitional stage (Seguí-Simarro et al., 2004) and this has two profound effects on the phragmoplast microtubules: their numbers drop precipitously and the number of horned microtubule plus ends increases to ~80% (Fig. 3D, Fig. 4C). Another interesting finding is that, during all phragmoplast stages except the transitional stage (when 80% of the microtubules are disassembling), the proportion of microtubules with extended plus ends remains remarkably constant at 15-20% (Fig. 4A).

The extent to which phragmoplast microtubule plus ends interact with cell-plate membranes has yet to be determined. To address this question, we have analysed the distances between horned and blunt microtubule plus ends, respectively, and their nearest cell-plate membrane in all of our tomograms (Fig. 5A,B). As shown in Fig. 5A, the analysis did not detect any preferred distance between the horned microtubule plus ends and the cell-plate membrane. By contrast, such a spatial relationship is clearly evident in Fig. 5B, which illustrates the relative frequency of blunt microtubule plus ends at specific distances from cell-plate membrane. In particular, there is a pronounced peak in the frequency distribution at 30 nm. This finding suggests that about 30% of the blunt-ended microtubules terminate at a distance of ~30 nm from a cell-plate membrane.

Fig. 2. (A) Serial 2.2 nm tomographic slice images (every third slice is shown) through the plus ends of a horned microtubule in which the protofilaments (arrowheads) are curling, characteristic of a disassembling microtubule. (B-M) Tomographic images and 3D models of reconstructed microtubule plus ends collected from all stages of phragmoplast development. (B-D′) Tomographic slices and corresponding models of blunt-ended microtubules. The blunt end architecture is somewhat variable, with one side often being slightly longer. (E-G′) Tomographic slices and corresponding models of microtubules with extended ends. (H-I′) Tomographic slices and corresponding models of horned microtubules. (J,J′) Tomographic slice and corresponding model of a microtubule with a hybrid (horned/extended) end. (K-M′) Tomographic slices and corresponding models of microtubules with flared ends. Because the thickness of a tomographic slice is 2.2 nm and the thickness of a protofilament ~4 nm, we were unable to model each protofilament individually. Therefore, the architecture is 'relatively mapped' and not all of the microtubules modeled exhibit 13 protofilaments. Color coding of the different microtubule plus-end types: blunt-ended, yellow; extended, green; horned, red; flared, blue; hybrid extended/horned, orange. Scale bars, 0.05 μm.

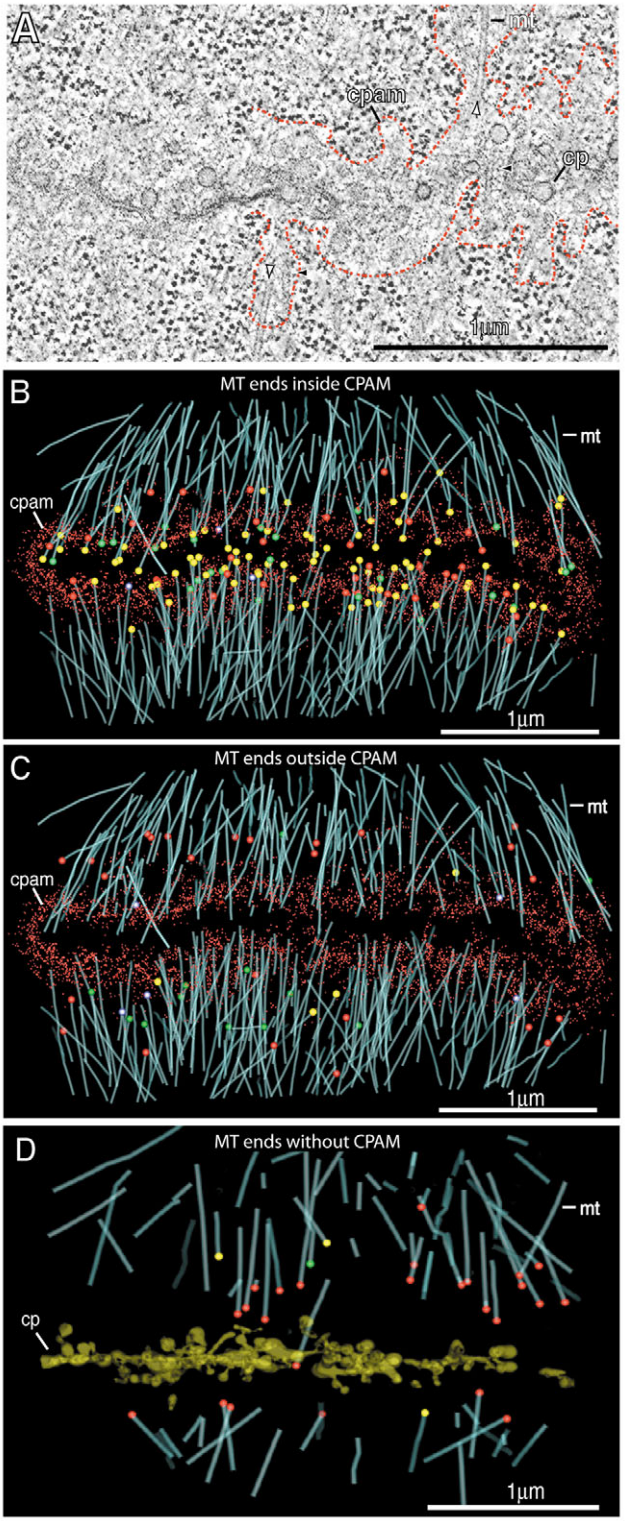

Fig. 3. (A) Projection of five consecutive 2.2 nm tomographic images of cell-plate-associated microtubule plus ends in a root-meristem cell (solid-phragmoplast stage). The black and white arrowheads point to morphologically different plus ends of microtubules. The dashed red line on the right-hand half of the image indicates the interface between the ribosome-rich cytosol and the ribosome-depleted cell-plate assembly matrix region. None of the microtubule plus ends pass across the cell-plate midline. (B-D) Mapping of microtubule plus end types, cell-plate assembly matrix (outlined with small red points) and microtubules (light blue). Color coding of the different microtubule plus-end types: blunt-ended, yellow; extended, green; horned, red; flared, blue. (B) A tomographic model of a solid phragmoplast from a shoot-meristem cell, showing all of the microtubules and the cell-plate assembly matrix outline; only microtubules whose plus ends are found within the cell-plate assembly matrix are color coded. (C) The same solid-phragmoplast tomographic models as shown in B, except that only microtubules whose plus ends are located outside the cell-plate assembly matrix are color coded. (D) A transitional phragmoplast from a root meristem. This tomographic model shows all of the microtubules but notice that this stage of phragmoplast development does not have a cell-plate assembly matrix. Color coding of microtubules' plus ends (see also Fig. 2): blunt, yellow; extended, green; horned, red; flared, blue. Notice the high proportion of blunt-ended microtubules that terminate within the cell-plate assembly matrix and the high proportion of horned microtubules that terminate outside a cell-plate assembly matrix. A quantitative analysis of the microtubule end types is presented in Fig. 4. Scale bars, 1 μm.

Discussion

Light-microscopy studies of living cells have shown that the phragmoplast microtubule array is a highly dynamic structure within which the microtubules turn over rapidly (Hush et al., 1994). So, there has been no accounting for the dynamics of individual microtubules within this array. To address this question, we have preserved *A. thaliana* root and shoot meristem cells using high-pressure-freezing/freeze-substitution techniques and then analysed the plastic-embedded samples using electron tomography. This approach has enabled us to obtain quantitative information about the microtubules within the different phragmoplast microtubule arrays and, in particular, about the microtubule plus-end morphologies and their association with the cell-plate assembly matrix. The four principal findings are: (1) microtubules do not interdigitate at the cell-plate mid-line; (2) the identification of five different types of microtubule plus-end morphology; (3) the demonstration that the association of the microtubule plus ends with the cell-plate assembly matrix alters the ratio of the different end types; and (4) the demonstration that about 30% of the blunt-ended microtubules terminate ~30 nm from a cell-plate membrane.

Phragmoplast microtubules do not interdigitate at the cell-plate mid-line during somatic-type cytokinesis

During the past 40 years, studies have come to different conclusions concerning the extent of microtubule interdigitation at the cell-plate mid-line during somatic-type cytokinesis (Pickett-Heaps and Northcote, 1966; Whaley et al., 1966; Hepler and Newcomb, 1967; Hepler and Jackson, 1968; Asada et al., 1991; Samuels et al., 1995; Müller et al., 2004; Van Damme et al., 2004). Nevertheless, it is generally assumed that phragmoplast microtubules do interdigitate, as in the depiction of somatic-type phragmoplasts with interdigitating microtubules in textbooks (Raven et al., 1999; Alberts et al., 2004). In the current study, we have not observed any examples of interdigitating phragmoplast microtubules in apical-meristem cells of *Arabidopsis*. The clearest evidence for interdigitating phragmoplast microtubules can be found in the

papers by Bajer (Bajer, 1968), Hepler and Jackson (Hepler and Jackson, 1968), Euteneuer et al. (Euteneuer et al., 1982), Brown and Lemmon (Brown and Lemmon, 1992), and Otegui et al. (Otegui et al., 2001). Common to all of these studies is that they described the events associated with syncytial-type cell-plate formation in endosperm cells and not somatic-type cell-plate formation in meristem cells. As discussed below, we have found no conclusive evidence in the plant cytokinesis literature for interdigitating phragmoplast microtubules during somatic-type cytokinesis. Thus, syncytial-type cytokinesis in plants differs from somatic-type cytokinesis not only in the geometry of cell-plate assembly intermediates (Otegui et al., 2001) but apparently also in the organization of the phragmoplast microtubules at the cell-plate mid-line.

During the course of this study of somatic-type cytokinesis in *Arabidopsis*, we analysed 16 tomograms (~9000 slice images) of phragmoplasts at various stages of cytokinesis, as well as >2000 electron micrographs of thinly sectioned cryogenically fixed cells. In none of these images did we find evidence for interdigitating microtubule plus ends. Nine out of 1123 microtubules (~0.8%) were found to cross the cell-plate mid-line but none were organized into close pairs or bundles. These results are consistent with findings of many earlier electron-microscope studies of somatic-type cell-plate formation (Pickett-Heaps and Northcote, 1966; Whaley et al., 1966; Hepler and Newcomb, 1967; Samuels et al., 1995).

Many excellent light-microscope analyses of somatic-type cell-plate formation using fluorescent tubulin antibodies (Gunning, 1982; Asada et al., 1991; Gu and Verma, 1997; Muller et al., 2004), injected fluorescent tubulin (Zang and Hepler, 1990; Hush et al., 1994) or green-fluorescent-protein-tagged tubulin in living cells (Ueda et al., 2003) have also failed to provide evidence for interdigitating phragmoplast microtubules. However, because most of the authors have

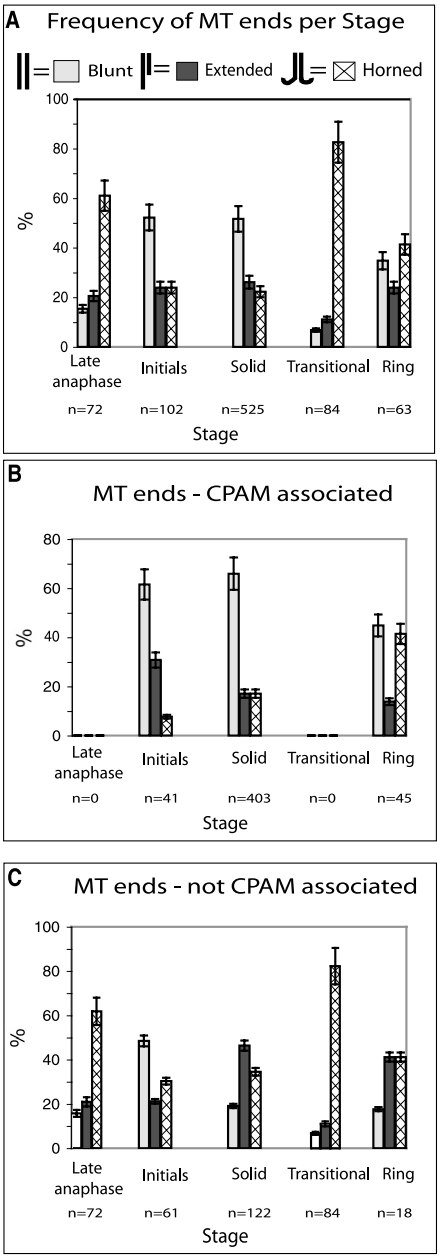

Fig. 4. Quantitative analysis of the plus-end types of cell-plate-associated microtubules. At each stage, three different cells were analysed, except for the solid-phragmoplast stage, for which four cells were analysed. (A) Percentages of microtubule plus-end types seen at each stage of cytokinesis. (B) Percentage of microtubule plus-end types that end within a cell-plate assembly matrix. (C) Percentages of microtubule plus ends that do not terminate within a cell-plate assembly matrix. *n*, number of microtubules counted in each stage.

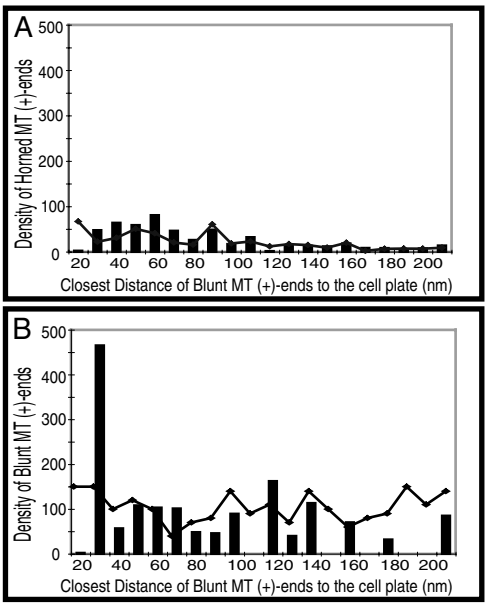

Fig. 5. Closest-approach analysis of horned (A) and blunt (B) microtubule plus ends to a cell-plate membrane. Solid-phragmoplast-stage cells from shoot and root meristems were examined for this analysis. The bars compose histograms of the actual densities of plus ends of microtubules at different distances from the cell-plate membrane. The line is the density distribution of plus ends of randomly distributed microtubules from the cell-plate membrane. (B) There is a significant peak in the distribution of blunt ends at 30 nm. This population is much greater than the calculated random distribution (thin line) than in A, which lacks such a peak. This suggests that about 30% of blunt-ended microtubules end at ~30 nm from the cell-plate membrane.

attempted to interpret their findings according to the interdigitating-microtubule model, the lack of fluorescence has been postulated to be due to inaccessibility of the probes to the interdigitating-microtubule region. Contradicting this explanation is the finding that the interdigitating microtubules of syncytial-type phragmoplasts can be fluorescently labeled across the mid-line (Nguyen et al., 2001).

When interpreting fluorescent microscope images, it should be remembered that their 3D resolution is 150-200 nm, whereas the resolution of our tomograms is ~7 nm. As illustrated in Fig. 6A, the width of the cell-plate matrix region is ~150 nm (i.e. close to the limit of resolution of the light microscope). To illustrate this point, we have calculated the equivalent fluorescent image of our tomographic reconstruction, displaying the individual microtubules as ~150 nm, slightly transparent objects (Fig. 6B). The similarity of this modeled image to published micrographs of fluorescently labeled somatic-type phragmoplasts is striking [compare Fig. 6B with published images (Gunning, 1982; Zang and Hepler, 1990; Asada et al., 1991; Hush et al., 1994; Gu and Verma, 1997; Ueda et al., 2003; Muller et al., 2004)].

Why do syncytial-type but not somatic-type phragmoplasts have interdigitating microtubule plus ends? We postulate that the syncytial-type phragmoplasts have interdigitating microtubules to help to stabilize their (mini)phragmoplasts mechanically, which consist of only about ten microtubules, as opposed to >1000 in somatic-type phragmoplasts (Hepler and Newcomb, 1967; Gunning, 1982; Otegui et al., 2001). Furthermore, the problem of phragmoplast stabilization is even more important during syncytial-type cytokinesis, because the simultaneous production of about six syncytial walls requires much more time (>1 hour) (Otegui and Staehelin, 2001) than the formation of one somatic-type cross-wall (10-20 min) (Zhang et al., 1990; Ueda et al., 2003).

Microtubules involved in cytokinesis and the phragmoplast exhibit three major and two minor geometries

In this study, which reports the characterization of the plus ends of 846 microtubules that were tracked end to end, we describe five different end types that are seen in all stages (Fig. 2). Three of these (blunt, extended and horned) correspond to the microtubule end types observed in vitro (Mandelkow et al., 1991; Chrétien et al., 1995; Carvalho et al., 2003). The flared end type appears to correspond to the flared type of kinetochore-associated microtubule plus end seen in *C. elegans* (O'Toole at al., 2003). The fifth, novel plus-end type (the hybrid type) shows an extended configuration on one side and a horned configuration on the other. Microtubules with flared ends (Fig. 2K-M′) and hybrid horned/extended ends (Fig. 2J,J′) are seen rather infrequently (flared type, 1-2%; hybrid type, <1%). This fact, together with the geometries of these two microtubule plus-end types, suggests that they correspond to transient microtubule plus-end states. Thus, the hybrid end type might correspond to a rescue or to a catastrophe event. More interesting is the 'coned' architecture of the flared ends (Fig. 2K′,L′,M′), which probably represents a transition between a blunt-ended, metastable microtubule and a disassembling, horned microtubule. This type of flared plus end has been reported to account for ~70% of the microtubules

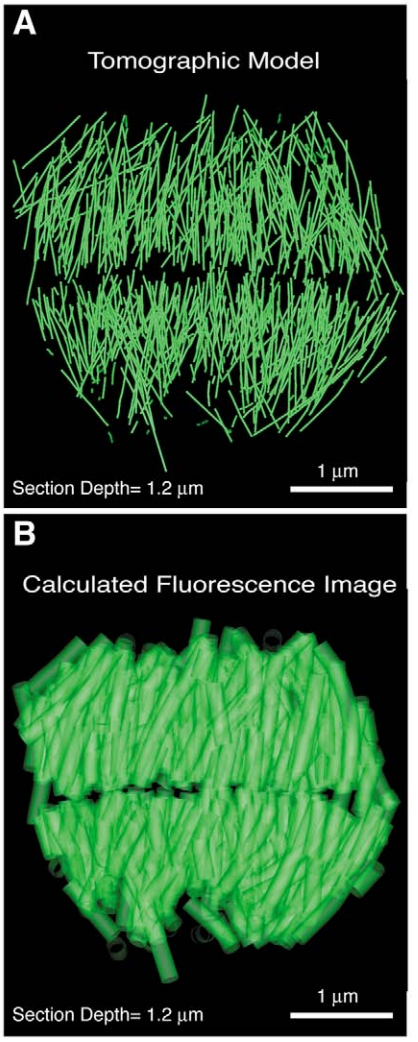

Fig. 6. Tomographic models showing a solid phragmoplast from a root-meristem cell. (A) Tomographic model with a section depth of 1.2 μm and with the microtubules (green) shown with their actual diameter of 25 nm. (B) Calculated fluorescence image based on the same tomographic model as in A. To produce this image, we increased the diameter of the microtubules to 150 nm (the limit of resolution of fluorescence-microscopy images) and made the microtubules look slightly transparent.

plus ends within the kinetochores of *C. elegans* (O'Toole et al., 2003), whereas, in this study of plant phragmoplast microtubules, <2% exhibited flared ends. This difference suggests that the geometry or the energetic properties of the flared microtubules plus-end configuration might be exploited by the kinetochore apparatus to help drive chromosome movement during mitosis.

Cell-plate assembly matrix stabilizes the plus ends of phragmoplast microtubules

The phragmoplast microtubule array is reorganized several times during cytokinesis (Lambert, 1993; Granger and Cyr, 2000; Mayer and Jürgens, 2004). Thus, understanding the functional relationship between microtubules and the cell-plate

assembly matrix within which the cell plate is formed is of central importance to understanding the mechanism of plant cell cytokinesis. Because the dynamic state of a microtubule plus end can be deduced from its geometry (Arnal et al., 2000; O'Toole et al., 2003), analysis of the types and frequencies of microtubule plus ends in cryogenically fixed and freeze-substituted cells can yield insights into the dynamic state of specific microtubule arrays. We have used this approach to evaluate the effect of the cell-plate assembly matrix on phragmoplast microtubule dynamics. The high proportion of cell-plate-assembly-matrix-associated microtubule plus ends with a blunt, metastable morphology (50-70%, Fig. 3B, Fig. 4B) contrasts greatly with the low proportion of such ends (5-50%) on microtubules that are not associated with the cell-plate assembly matrix (Fig. 3C,D, Fig. 4C). In fact, these microtubules that are not associated with the cell-plate assembly matrix exhibit a much higher proportion of horned, disassembling microtubule plus ends (30-80%) than those within the matrix (5-40%). Because blunt-ended microtubules are metastable, we conclude that the cell-plate assembly matrix contains molecules that help stabilize phragmoplast microtubule plus ends. This results in a reduced rate of turnover of phragmoplast microtubules that are optimally organized to deliver the Golgi-derived vesicles to the growing cell plate.

Some phragmoplast microtubules terminate ~30 nm from a cell-plate membrane

As reported previously (Seguí-Simarro et al., 2004), the phragmoplast microtubules that terminate within the cell-plate assembly matrix rarely extend beyond the equatorial cell plate (Fig. 1, Fig. 3A). Similarly, when the tips of extended (growing) microtubules are traced in tomograms, they often stop at the level of the cell plate (Fig. 3). Together, these observations suggest that molecules associated with the cell-plate membranes might be able to capture the tips of growing microtubules and to stop their growth. Total internal reflection fluorescence (TIRF) microscopy studies of fibroblasts have demonstrated that microtubule plus ends can be captured <50 nm from the plasma membrane (Small and Kaverina, 2003). With this finding in mind, we analysed the distances between the ends of both blunt and horned microtubules, and cell-plate membranes in all of our tomograms. The analysis demonstrated that about one-third of the blunt-ended microtubules terminate ~30 nm from a cell-plate membrane (Fig. 5A), whereas no preferential distance was observed for the horned microtubule plus ends (Fig. 5B) or extended microtubule plus ends (data not shown). This finding indicates that, during somatic-type cytokinesis, a significant proportion of the blunt-ended (metastable) phragmoplast microtubules could be connected to cell-plate membranes via linker molecules. The presence of such molecules would explains why Kakimoto and Shibaoka (Kakimoto and Shibaoka, 1992) were able to isolate intact phragmoplasts (cell plates with opposing sets of microtubules) from dividing *Nicotiana tabacum* BY-2 cells and why cell-plate-associated microtubules and actin filaments became misaligned as a unit by myosin-disrupting agents (Molchan et al., 2002).

At present, the identities of postulated phragmoplast microtubule plus-end capture proteins are unknown. The *Arabidopsis* genome contains three EB1-encoding and nine MAP65-encoding genes (Mathur et al., 2003; Müller et al., 2004). Of these, AtEB1 appears to be the best candidate for being part of a microtubule plus-end capture complex because it is the only one that has been localized to the growing plus ends of microtubules (Mathur et al., 2003; Van Damme et al., 2004). This suggestion contradicts the hypothesis of Van Damme et al., who proposed that AtMap65-3, which has been localized to the phragmoplast mid-line by fluorescence labeling (Müller et al., 2004; Van Damme et al., 2004), binds to overlapping phragmoplast microtubule regions and stabilizes the microtubules. Given the absence of overlapping microtubules in our tomographic models and the ~200 nm limit of resolution of fluorescence microscopy, we suggest that the hypothesis that AtMAP65-3 binds to overlapping microtubules should be abandoned. Instead, the finding that a mutation in the microtubule-binding domain of *AtMAP65-3* leads to a characteristic widening of the microtubule-depleted mid-line region of the phragmoplast (Müller et al., 2004), is consistent with the idea that this protein is part of a plus-end capture complex.

We thank M. S. Otegui, B.-H. Kang and B. S. Donohoe for helpful conversations about this work, R. McIntosh for critical reading of the manuscript and P. K. Hepler for critical review of the figures. D. Mastronarde and R. Gaudette provided essential application software. This work was supported by the National Institute of Health Grant GM59787 to L.A.S.

References

Alberts, B., Bray, D., Hopkin, K., Johnson, A., Lewis, J., Raff, M., Roberts, K. and Walter, P. (2004). Essential cell biology. In *Cell Division*, 2nd edn, pp. 637-658. New York: Garland Science.

Arnal, I., Karsenti, E. and Hyman, A. A. (2000). Structural transitions at microtubule ends correlate with their dynamic properties in *Xenopus* egg extracts. *J. Cell Biol.* **149**, 767-774.

Asada, T., Sonobe, S. and Shibaoka, H. (1991). Microtubule translocation in the cytokinetic apparatus of cultured tobacco cells. *Nature* **350**, 238-241.

Bajer, A. S. (1968). Fine structure studies on phragmoplast and cell plate formation. *Chromosoma* **24**, 238-417.

Brown, R. C. and Lemmon, B. E. (1992). Control of division plane in normal and Griseofulvin-treated microsporocytes of magnolia. *J. Cell Sci.* **103**, 1031-1038.

Carvalho, P., Tirnauer, J. S. and Pellman, D. (2003). Surfing on microtubule ends. *Trends Cell Biol.* **13**, 229-237.

Chretien, D., Fuller, S. D. and Karsenti, E. (1995). Structure of growing microtubule ends – 2-dimensional sheets close into tubes at variable rates. *J. Cell Biol.* **129**, 1311-1328.

Euteneuer, U., Jackson, W. T. and McIntosh, J. R. (1982). Polarity of spindle microtubules in *Haemanthus* endosperm. *J. Cell Biol.* **94**, 644-653.

Gilbert, P. F. C. (1972). Reconstruction of a 3-dimensional structure from projections and its application to electron-microscopy II. *Proc. R. Soc. London B Biol. Sci.* **182**, 89-102.

Granger, C. L. and Cyr, R. J. (2000). Microtubule reorganization in tobacco BY-2 cells stably expressing GFP-MBD. *Planta* **210**, 502-509.

Gu, X. and Verma, D. P. S. (1997). Dynamics of phragmoplastin in living cells during cell plate formation and uncoupling of cell elongation from the plane of cell division. *Plant Cell* **9**, 157-169.

Gunning, B. E. S. (1982). The cytokinetic apparatus: its development and spatial regulation. In *The Cytoskeleton in Plant Growth and Development* (ed. C. W. Lloyd), pp. 229-292. London: Academic Press.

Gunning, B. E. S. and Steer, M. W. (1975). *Ultrastructure and Biology of Plant Cells*. London: Edward Arnold Publishers.

Hepler, P. K. and Newcomb, E. H. (1967). Fine structure of cell plate formation in the apical meristem of *Phaseolus* roots. *J. Ultrastruct. Res.* **19**, 498-513.

Hepler, P. K. and Jackson, W. T. (1968). Microtubules and early stages of cell-plate formation in the endosperm of *Haemanthus katherinea* Baker. *J. Cell Biol.* **38**, 437-446.

Hush, J. M., Wadsworth, P., Callaham, D. A. and Hepler, P. K. (1994). Quantification of microtubule dynamics in living plant cells using fluorescence redistribution after photobleaching. *J. Cell Sci.* **107**, 775-784.

Kakimoto, T. and Shibaoka, H. (1992). Synthesis of polysaccharides in phragmoplasts isolated from tobacco BY-2 cells. *Plant Cell Physiol.* **33**, 353-361.

Kremer, J. R., Mastronarde, D. N. and McIntosh, J. R. (1996). Computer visualization of three-dimensional image data using IMOD. *J. Struct. Biol.* **116**, 71-76.

Ladinsky, M. S., Kremer, J. R., Mastronarde, D. N., McIntosh, J. R., Staehelin, L. A. and Howell, K. E. (1997). HVEM tomography of the Golgi ribbon in cryofixed NRK cells: The non-compact region, the CGN and TGN. *Mol. Biol. Cell Suppl.* **8**, 2040.

Ladinsky, M. S., Mastronarde, D. N., McIntosh, J. R., Howell, K. E. and Staehelin, L. A. (1999). Golgi structure in three dimensions: functional insights from the normal rat kidney cell. *J. Cell Biol.* **144**, 1135-1149.

Lambert, A.-C. (1993). Microtubule-organizing centers in higher plants. *Curr. Opin. Cell Biol.* **5**, 116-122.

Mandelkow, E.-M., Mandelkow, E. and Milligan, R. A. (1991). Microtubule dynamics and microtubule caps: a time-resolved cryo-electron microscopy study. *J. Cell Biol.* **114**, 977-991.

Marsh, B. J., Mastronarde, D. N., Buttle, K. F., Howell, K. E. and McIntosh, J. R. (2001). Organellar relationships in the Golgi region of the pancreatic beta cell line, HIT-T15, visualized by high resolution electron tomography. *Proc. Natl. Acad. Sci. USA* **98**, 2399-2406.

Mastronarde, D. N. (1997). Dual-axis tomography: an approach with alignment methods that preserve resolution. *J. Struct. Biol.* **120**, 343-352.

Mathur, J., Mathur, N., Kernebeck, B., Srinivas, B. P. and Hulskamp, M. (2003). A novel localization pattern for an EB1-like protein links microtubule dynamics to endomembrane organization. *Curr. Biol.* **13**, 1991-1997.

Mayer, U. and Jurgens, G. (2004). Cytokinesis: lines of division taking shape. *Curr. Opin. Plant Biol.* **7**, 599-604.

Molchan, T. M., Valster, A. H. and Hepler, P. K. (2002). Actomyosin promotes cell plate alignment and late lateral expansion in *Tradescantia* stamen hair cells. *Planta* **214**, 683-693.

Müller, S., Smertenko, A., Wagner, V., Heinrich, M., Hussey, P. J. and Hauser, M. T. (2004). The plant microtubule-associated protein AtMAP65-3/PLE is essential for cytokinetic phragmoplast function. *Curr. Biol.* **14**, 412-417.

Nguyen, H., Brown, R. C. and Lemmon, B. E. (2001). Patterns of cytoskeletal organization reflect distinct developmental domains in endosperm of *Coronopus didymus* (Brassicaceae). *Int. J. Plant Sci.* **162**, 1-14.

O'Toole, E. T., McDonald, K. L., Mantler, J., McIntosh, J. R., Hyman, A. A. and Muller-Reichert, T. (2003). Morphologically distinct microtubule ends in the mitotic centrosome of *Caenorhabditis elegans*. *J. Cell Biol.* **163**, 451-456.

Otegui, M. S. and Staehelin, L. A. (2000). Cytokinesis in flowering plants: more than one way to divide a cell. *Curr. Opin. Cell Biol.* **3**, 493-502.

Otegui, M. S., Mastronarde, D. N., Kang, B. H., Bednarek, S. Y. and Staehelin, L. A. (2001). Three-dimensional analysis of syncytial-type cell plates during endosperm cellularization visualized by high resolution electron tomography. *Plant Cell* **13**, 2033-2051.

Pickett-Heaps, J. D. and Northcote, D. H. (1966). Organization of microtubules and endoplasmic reticulum during mitosis and cytokinesis in wheat meristems. *J. Cell Sci*. **1**, 109-120.

Raven, P. H., Evert, R. F. and Eichhorn, S. E. (1999). The reproduction of cells. In *Biology of Plants*, 6th edn, pp. 155-167. New York: W. H. Freeman and Company/Worth.

Samuels, A. L., Giddings, T. H. and Staehelin, L. A. (1995). Cytokinesis in tobacco BY-2 and root-tip cells – a new model of cell plate formation in higher-plants. *J. Cell Biol.* **130**, 1345-1357.

Segui-Simarro, J. M., Austin, J. R., White, E. A. and Staehelin, L. A. (2004). Electron tomographic analysis of somatic cell plate formation in meristematic cells of *Arabidopsis* preserved by high-pressure freezing. *Plant Cell* **16**, 836-856.

Small, J. V. and Kaverina, I. (2003). Microtubules meet substrate adhesions to arrange cell polarity. *Curr. Opin. Cell Biol.* **15**, 40-47.

Smertenko, A. P., Chang, H. Y., Wagner, V., Kaloriti, D., Fenyk, S., Sonobe, S., Lloyd, C., Hauser, M. T. and Hussey, P. J. (2004). The Arabidopsis microtubule-associated protein AtMAP65-1: molecular analysis of its microtubule bundling activity. *Plant Cell* **16**, 2035-2047.

Staehelin, L. A. and Hepler, P. K. (1996). Cytokinesis in higher plants. *Cell* **84**, 821-824.

Ueda, K., Sakaguchi, S., Kumagai, F., Hasezawa, S., Quader, H. and Kristen, U. (2003). Development and disintegration of phragmoplasts in living cultured cells of a *GFP::TUA6* transgenic *Arabidopsis thaliana* plant. *Protoplasma* **220**, 111-118.

Van Damme, D., Bouget, F.-Y., Poucke, K. V., Inze, D. and Geelen, D. (2004). Molecular dissection of plant cytokinesis and phragmoplast structure: a survey of GFP-tagged proteins. *Plant J.* **40**, 386-398.

Verma, D. P. S. (2001). Cytokinesis and building of the cell plate in plants. *Annu. Rev. Plant Physiol. Plant Mol. Biol*. **52**, 751-784.

Wasteneys, G. O. (2002). Microtubule organization in the green kingdom: chaos or self-order? *J. Cell Sci.* **115**, 1345-1354.

Whaley, W. G., Dauwalder, M. and Kephart, J. E. (1966). The Golgi apparatus and an early stage in cell plate formation. *J. Ultrastruct. Res.* **15**, 169-180.

Wick, S. M., Muto, S. and Duniec, J. (1985). Double immunofluorescence labeling of calmodulin and tubulin in dividing plant-cells. *Protoplasma* **126**, 198-206.

Zhang, D., Wadsworth, P. and Hepler, P. K. (1990). Microtubule dynamics in living dividing plant cells: confocal imaging of microinjected fluorescent brain tubulin. *Proc. Natl. Acad. Sci. USA* **87**, 8820-8824.